ELSEVIER

International Journal of Solids and Structures 41 (2004) 765–784

INTERNATIONAL JOURNAL OF SOLIDS and STRUCTURES

www.elsevier.com/locate/ijsolstr

Chaotic and asymmetrical beam response to impulsive load

Y.M. Liu [a], G.W. Ma [a,*], Q.M. Li [b]

[a] School of Civil and Environmental Engineering, Nanyang Technological University, Nanyang Avenue, Singapore 639798, Singapore
[b] Department of Mechanical, Aerospace and Manufacturing Engineering, UMIST, P.O. Box 88, Manchester M60 1QD, UK

Received 2 June 2003; received in revised form 21 September 2003

Abstract

Both symmetrical and asymmetrical final displacements are observed for elastic–plastic beams under symmetrical impulsive loading. A three-degree-of-freedom Shanley-type model is developed in this study, which is capable of revealing chaotic and asymmetrical responses of an elastic–plastic beam by introducing initial imperfections. To identify the asymmetrical displacement, the beam response is decomposed into three vibration modes. Corresponding modal participation factors are derived based on the displacement of the three-degree-of-freedom beam model. Phase plane trajectories, Poincaré maps and power spectral density diagrams are derived to illustrate both the symmetrical and asymmetrical chaotic vibrations. Numerical simulations using a general-purpose FE code LS-DYNA are carried out for an elastic–plastic beam subjected to impulsive load. The simulation results indicate that the elastic–plastic beam demonstrates chaotic and asymmetrical vibration when the applied impulsive load exceeds a critical value, which agrees with experimental observations.

Keywords: Chaotic and asymmetrical response; Impulsive load; Three-degree-of-freedom beam model; Elastic–plastic beam

1. Introduction

The counter-intuitive phenomenon refers to the observation that the final midspan point of elastic–plastic beams rests in the same side of the applied load. Symonds and Yu (1985) firstly observed this phenomenon when modeling the dynamic response of an elastic–plastic beam subjected to impulsive load. This phenomenon has been proven by independent impact experiments on thin elastic–plastic beams by Li et al. (1991) and Kolsky et al. (1991), respectively. Similar phenomenon was also detected for elastic–plastic plates and shells in underwater and air explosions (Galiev, 1996, 1997). A single-degree-of-freedom (1-DoF) Shanley-type beam model was developed to capture the basic features of the counter-intuitive response and identify the intrinsic mechanism (Symonds and Yu, 1985; Genna and Symonds, 1987; Symonds et al., 1986). The Shanley model was later extended to two-degree-of-freedom (2-DoF) for further illustration of the chaotic unpredictability, strain energy distribution, and damping effect (Lee and Symonds, 1992; Lee

* Corresponding author. Tel.: +65-67904984; fax: +65-67910676.
E-mail address: cgwma@ntu.edu.sg (G.W. Ma).

0020-7683/$ - see front matter © 2003 Elsevier Ltd. All rights reserved.
doi:10.1016/j.ijsolstr.2003.09.048

et al., 1992). Except the Shanley-type beam model, Qian and Symonds (1996) developed a Galerkin beam model to explore the anomalous beam dynamics, and the results were compared with the FE solutions. Similar Galerkin models of finite degrees of freedom were developed to study the anomalous response of elastic–plastic circular plates (Bassi et al., 2002). It has been concluded that the counter-intuitive response is a type of extremely parameter-sensitive phenomenon, which is accompanied with chaotic vibration and anomalous final displacement of the beams (Li et al., 1991; Lee and Symonds, 1992; Li and Liu, 2003). Evidence of chaos for elastic, plastic beams under short pulse load has been observed in displacement–time histories, phase plane trajectories, Poincaré maps, power spectral density diagrams and Lyapunov exponents (Lee and Symonds, 1992).

However, with the available 1-DoF and 2-DoF Shanley-type models (Symonds and Yu, 1985; Lee et al., 1992), only symmetrical displacements of the beam can be approached. Asymmetrical displacement has been ignored in all the previous analytical and numerical studies although Li et al. (1991) reported not only the counter-intuitive behavior but also asymmetrical final displacements of thin clamped beams. The existing symmetrical models are unable to capture the asymmetrical displacements.

In the present study, a three-degree-of-freedom (3-DoF) Shanley-type model is developed for elastic–plastic beam, which captures symmetrical and asymmetrical chaotic responses. The 2-DoF Shanley-type model (Lee et al., 1992), considered as a special case of the 3-DoF model, is used for the benchmark test of the present model where asymmetrical vibration may be activated by applying very small initial imperfection of the beam. The derived beam response is decomposed into three vibration modes. The corresponding modal participation factors enable to illustrate clearly the chaotic behavior of both symmetrical and asymmetrical responses. An elastic–plastic uniform beam is also analyzed by using a general-purpose FE code LS-DYNA, which confirms that elastic–plastic beam does demonstrate chaotic and asymmetrical vibration when the applied impulsive load exceeds a critical value. In consideration that the counter-intuitive phenomenon is the first order chaotic response, the anomalous asymmetrical final displacement can be interpreted as the second order chaotic response of elastic–plastic thin beam subject to impulsive load.

2. Three-degree-of-freedom analytical model

The 3-DoF Shanley-type beam model is illustrated schematically in Fig. 1. *AB*, *BC*, *CD* and *DE* are rigid bars of mass $m/2$ ($2m$ represents the total mass of the beam) connected to deformable zero-length 'cells' at *B*, *C* and *D*, which are assumed to act as sandwich beam sections (Symonds and Yu, 1985; Lee et al., 1992). The vertical displacements at the left-quarter point *B*, the midpoint *C* and the right-quarter point *D* are denoted as w_1, w_2 and w_3, respectively. The corresponding horizontal displacements at these three points are u_1, u_2 and u_3. The force acting at the midpoint is a rectangular pulse. Superior to those symmetrical half-beam models, the present 3-DoF model is capable of catching the asymmetrical transverse deformations.

As shown in Fig. 1, the stresses in the 'cells' at *B* and *D* are indicated by σ_{B1}, σ_{B2}, σ_{D1} and σ_{D2}, where the subscripts 1 and 2 refer to the upper and lower flanges, respectively. The 'cell' at *C* is divided into two parts along the vertical axis through the midpoint. The stresses in the left half are denoted by σ_{C1} and σ_{C2}, those in the right half σ_{C3} and σ_{C4}, where the subscripts 1, 3 and 2, 4 refer to the upper and lower flanges, respectively. The material is assumed to be elastic, perfectly plastic. The yielding conditions and flow rules are as follows:

$$-\sigma_0 \leqslant \sigma_{\alpha i} \leqslant \sigma_0 \tag{1}$$

$$(\sigma_{\alpha i} \pm \sigma_0)\, \mathrm{d}\varepsilon^p_{\alpha i} \geqslant 0 \tag{2}$$

where $i = 1, 2$ when $\alpha = B$ or D and $i = 1, 2, 3, 4$ when $\alpha = C$ (no summation over α and i). σ_0 is the yielding stress in each flange. The strain increments at each flange consist of elastic and plastic components, so that

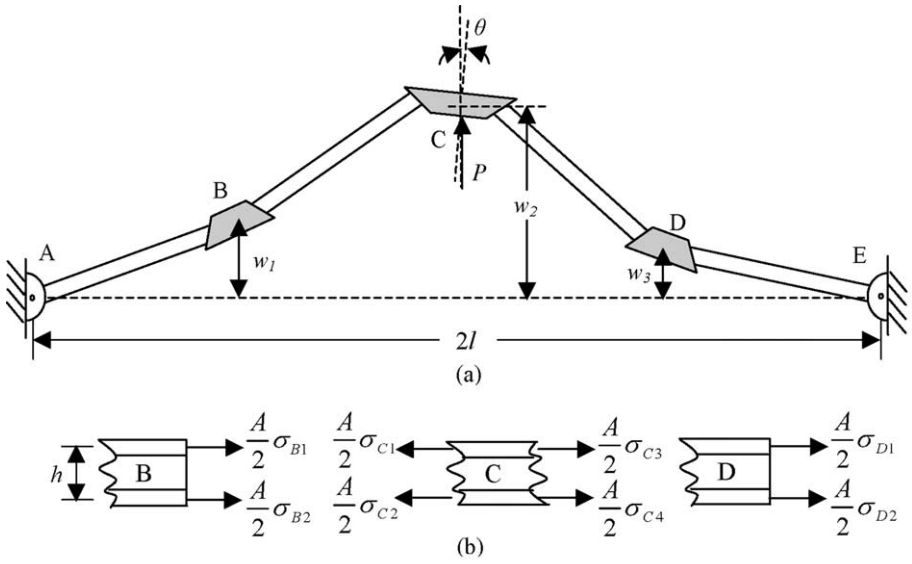

Fig. 1. Three-degree-of-freedom beam model: (a) deflected beam model; (b) deformable sandwich cells.

$$\mathrm{d}\varepsilon_{\alpha i} = \frac{1}{E}\,\mathrm{d}\sigma_{\alpha i} + \mathrm{d}\varepsilon^{p}_{\alpha i} \tag{3}$$

where E is the Young's modulus.

The stresses can be obtained by integrating Eq. (3):

$$\sigma_{\alpha i} = E(\varepsilon_{\alpha i} - \varepsilon^{p}_{\alpha i}) \tag{4}$$

According to the geometrical and stress–strain relationship, the stresses can be expressed as

$$\begin{Bmatrix} \sigma_{B1} \\ \sigma_{B2} \end{Bmatrix} = E\left(\left\{ \frac{2u_1}{l} + \frac{2w_1^2}{l^2} \pm \frac{2h}{l^2}(2w_1 - w_2) \right\} - \begin{Bmatrix} \varepsilon^{p}_{B1} \\ \varepsilon^{p}_{B2} \end{Bmatrix} \right) \tag{5}$$

$$\begin{Bmatrix} \sigma_{C1} \\ \sigma_{C2} \end{Bmatrix} = E\left(\left\{ -\frac{2u_1}{l} + \frac{2u_2}{l} + \frac{2(w_2 - w_1)^2}{l^2} \pm \frac{2h}{l^2}(w_2 - w_1) \right\} - \begin{Bmatrix} \varepsilon^{p}_{C1} \\ \varepsilon^{p}_{C2} \end{Bmatrix} \right) \tag{6}$$

$$\begin{Bmatrix} \sigma_{C3} \\ \sigma_{C4} \end{Bmatrix} = E\left(\left\{ -\frac{2u_2}{l} + \frac{2u_3}{l} + \frac{2(w_2 - w_3)^2}{l^2} \pm \frac{2h}{l^2}(w_2 - w_3) \right\} - \begin{Bmatrix} \varepsilon^{p}_{C3} \\ \varepsilon^{p}_{C4} \end{Bmatrix} \right) \tag{7}$$

$$\begin{Bmatrix} \sigma_{D1} \\ \sigma_{D2} \end{Bmatrix} = E\left(\left\{ -\frac{2u_3}{l} + \frac{2w_3^2}{l^2} \pm \frac{2h}{l^2}(2w_3 - w_2) \right\} - \begin{Bmatrix} \varepsilon^{p}_{D1} \\ \varepsilon^{p}_{D2} \end{Bmatrix} \right) \tag{8}$$

where

$$\frac{u_1}{l} = -\frac{3w_1^2}{4l^2} + \frac{w_3^2}{4l^2} + \frac{(w_2 - w_1)^2}{4l^2} + \frac{(w_2 - w_3)^2}{4l^2} + \frac{1}{16}(3\varepsilon^{p}_{B1} + 3\varepsilon^{p}_{B2} - \varepsilon^{p}_{C1} - \varepsilon^{p}_{C2} - \varepsilon^{p}_{C3} - \varepsilon^{p}_{C4} - \varepsilon^{p}_{D1} - \varepsilon^{p}_{D2}) \tag{9}$$

$$\frac{u_2}{l} = -\frac{w_1^2}{2l^2} + \frac{w_3^2}{2l^2} - \frac{(w_2 - w_1)^2}{2l^2} + \frac{(w_2 - w_3)^2}{2l^2} + \frac{1}{8}(\varepsilon^{p}_{B1} + \varepsilon^{p}_{B2} + \varepsilon^{p}_{C1} + \varepsilon^{p}_{C2} - \varepsilon^{p}_{C3} - \varepsilon^{p}_{C4} - \varepsilon^{p}_{D1} - \varepsilon^{p}_{D2}) \tag{10}$$

$$\frac{u_3}{l} = -\frac{w_1^2}{4l^2} + \frac{3w_3^2}{4l^2} - \frac{(w_2 - w_1)^2}{4l^2} - \frac{(w_2 - w_3)^2}{4l^2} + \frac{1}{16}(\varepsilon_{B1}^p + \varepsilon_{B2}^p + \varepsilon_{C1}^p + \varepsilon_{C2}^p + \varepsilon_{C3}^p + \varepsilon_{C4}^p - 3\varepsilon_{D1}^p - 3\varepsilon_{D2}^p) \tag{11}$$

It has been assumed during the manipulation of Eqs. (5)–(11) that the axial force is constant over the length of the beam by neglecting axial inertia effects.

The equations of motion for the system can be written in the following matrix form:

$$\frac{ml}{24}\begin{bmatrix} 4 & 1 & 0 \\ 0 & 1 & 4 \\ 1 & 4 & 1 \end{bmatrix}\begin{Bmatrix} \ddot{w}_1 \\ \ddot{w}_2 \\ \ddot{w}_3 \end{Bmatrix} + N\cos\theta \cdot \begin{bmatrix} 2 & -1 & 0 \\ 0 & -1 & 2 \\ -1 & 2 & -1 \end{bmatrix}\begin{Bmatrix} w_1 \\ w_2 \\ w_3 \end{Bmatrix} + \begin{bmatrix} 2 & -1 & 0 & 0 \\ 0 & 0 & -1 & 2 \\ -1 & 1 & 1 & -1 \end{bmatrix}\begin{Bmatrix} M_1 \\ M_2 \\ M_3 \\ M_4 \end{Bmatrix} = \begin{Bmatrix} 0 \\ 0 \\ \frac{Pl}{2} \end{Bmatrix} \tag{12}$$

where P is the external impulsive load characterized by a rectangular pulse load of intensity P and duration t_0 in the present study; θ is the rotation angle of cell C with an initial value of 0. It can be determined by combining the equilibrium equations of the right and left parts of the beam through considering the constant axial force in the beam. The rotation angle θ is normally very small because the transverse deflection is much smaller than the dimension of the beam span. In the present study, $\sin\theta$ has been eliminated in the equilibrium equation (12) when combining the equilibrium equations of the right and left parts, however, $\cos\theta$ in Eq. (12) is approximated to 1 in order to keep a linear form of the differential equations. The axial force and bending moment variables in Eq. (12) are obtained via the following equations:

$$N = \frac{AE}{2}\left[\frac{w_1^2}{l^2} + \frac{w_3^2}{l^2} + \frac{(w_2 - w_1)^2}{l^2} + \frac{(w_2 - w_3)^2}{l^2} - \frac{1}{4}(\varepsilon_{B1}^p + \varepsilon_{B2}^p + \varepsilon_{C1}^p + \varepsilon_{C2}^p + \varepsilon_{C3}^p + \varepsilon_{C4}^p + \varepsilon_{D1}^p + \varepsilon_{D2}^p)\right] \tag{13}$$

$$\begin{Bmatrix} M_1 \\ M_2 \\ M_3 \\ M_4 \end{Bmatrix} = AEh\left(\frac{h}{l^2}\begin{bmatrix} 2 & -1 & 0 \\ -1 & 1 & 0 \\ 0 & 1 & -1 \\ 0 & -1 & 2 \end{bmatrix}\begin{Bmatrix} w_1 \\ w_2 \\ w_3 \end{Bmatrix} - \frac{1}{4}\begin{Bmatrix} \varepsilon_{B1}^p - \varepsilon_{B2}^p \\ \varepsilon_{C1}^p - \varepsilon_{C2}^p \\ \varepsilon_{C3}^p - \varepsilon_{C4}^p \\ \varepsilon_{D1}^p - \varepsilon_{D2}^p \end{Bmatrix}\right) \tag{14}$$

It should be noted that the bending moments on cell C are not in balance, i.e., $M_2 \neq M_3$.

Substituting Eqs. (13) and (14) into Eq. (12), furnishes,

$$[\mathbf{M}]\{\ddot{\mathbf{w}}\} + [\mathbf{K}_1]\{\mathbf{w}\} + [\mathbf{K}_2]\{\mathbf{w}\} + [\mathbf{G}_1]\{\boldsymbol{\varepsilon}^p\} + \{\mathbf{G}_2\} = \{\mathbf{f}\} \tag{15}$$

where the matrices are

$$[\mathbf{M}] = \frac{m}{24EA}\begin{bmatrix} 4 & 1 & 0 \\ 0 & 1 & 4 \\ 1 & 4 & 1 \end{bmatrix}, \quad [\mathbf{K}_1] = \frac{h^2}{l^3}\begin{bmatrix} 5 & -3 & 0 \\ 0 & -3 & 5 \\ -3 & 4 & -3 \end{bmatrix}, \quad [\mathbf{K}_2] = \frac{1}{8l}\left(\sum \varepsilon^p\right)\begin{bmatrix} -2 & 1 & 0 \\ 0 & 1 & -2 \\ 1 & -2 & 1 \end{bmatrix},$$

$$[G_1] = \frac{h}{4l}\begin{bmatrix} -2 & 2 & 1 & -1 & 0 & 0 & 0 & 0 \\ 0 & 0 & 0 & 0 & 1 & -1 & -2 & 2 \\ 1 & -1 & -1 & 1 & -1 & 1 & 1 & -1 \end{bmatrix}$$

and the vectors are

$$\{\mathbf{w}\} = \begin{Bmatrix} w_1 \\ w_2 \\ w_3 \end{Bmatrix}, \quad \{\mathbf{f}\} = \begin{Bmatrix} 0 \\ 0 \\ \frac{P}{2AE} \end{Bmatrix}, \quad \{\varepsilon^p\} = [\,\varepsilon^p_{B1} \quad \varepsilon^p_{B2} \quad \varepsilon^p_{C1} \quad \varepsilon^p_{C2} \quad \varepsilon^p_{C3} \quad \varepsilon^p_{C4} \quad \varepsilon^p_{D1} \quad \varepsilon^p_{D2}\,]'$$

$$[G_2] = \frac{1}{2l^3} \begin{Bmatrix} (2w_1 - w_2)\left[w_1^2 + w_3^2 + (w_2 - w_1)^2 + (w_2 - w_3)^2\right] \\ (-w_2 + 2w_3)\left[w_1^2 + w_3^2 + (w_2 - w_1)^2 + (w_2 - w_3)^2\right] \\ (-w_1 + 2w_2 - w_3)\left[w_1^2 + w_3^2 + (w_2 - w_1)^2 + (w_2 - w_3)^2\right] \end{Bmatrix}$$

in which $\sum \varepsilon^p = \varepsilon^p_{B1} + \varepsilon^p_{B2} + \varepsilon^p_{C1} + \varepsilon^p_{C2} + \varepsilon^p_{C3} + \varepsilon^p_{C4} + \varepsilon^p_{D1} + \varepsilon^p_{D2}$; $A/2$ is the area of each flange; h is the distance between the flanges of each cell; and an overhead dot denotes the time derivatives. Eq. (15) contains both material and geometrical nonlinear terms. Material and geometrical parameters of the model are selected as $\sigma_0 = 0.3$ GPa, $E = 40$ GPa, $m = 0.0216$ kg, $l = 0.1$ m, $A = 8 \times 10^{-5}$ m^2, and $h = 2.71 \times 10^{-3}$ m. The duration for the short pulse is $t_0 = 0.5$ ms throughout the analysis, whereas the magnitude of the pulse is variable. The parameters employed in the present study are exactly the same as those used by Lee et al. (1992).

3. Symmetrical response

Eq. (15) is then integrated numerically using central finite difference method. The time step is adopted as $\mathrm{d}t = 0.5 \times 10^{-7}$ s. Justification of the time step for convergence of finite difference method has been discussed in Lee et al. (1992). Trial-and-error method is further used in the present study to justify the convergence for the adopted time step. In each time step the yielding condition is examined and appropriate stress–strain relationship is used.

The present 3-DoF model can be simplified into the 2-DoF model (Lee et al., 1992), if it is considered as an ideal symmetrical structure. The displacement–time histories for ideal symmetrical model at the midpoint C for $P = 1000$, 2800 and 4000 N are shown in Fig. 2. In Fig. 2(a) for $P = 1000$ N, the response is entirely elastic in spite of geometrical nonlinearity. It is a kind of quasi-periodic vibration with displacement varies in range of negative limit to equivalent positive limit. In Fig. 2(b) for $P = 2800$ N, after the initial rebounding period, it vibrates solely on the negative side, which is known as the counter-intuitive phenomenon. With $P = 4000$ N in Fig. 2(c), the midpoint displacement vibrates in alignment with the applied load after the impulsive load is removed, which returns back to the intuitively expected mode.

Detailed discussions on the chaotic response of the symmetrical beam model can be found in Lee and Symonds (1992) and Lee et al. (1992). The vibration pattern and magnitude obtained with the present 3-DoF Shanley-type beam model agree well with those reported previously (Lee et al., 1992), which validates the assumptions and equations in the present model.

4. Asymmetrical response

The symmetrical response is the only response mode for an ideal symmetrical model, e.g., 1-DoF and 2-DoF Shanley-type models. However, for any engineering structural problems, small perturbation due to geometrical and material imperfections, improperly applied loading and boundary conditions is inevitable, which may activate asymmetrical response mode of the system, as shown by experimental results in Li et al.

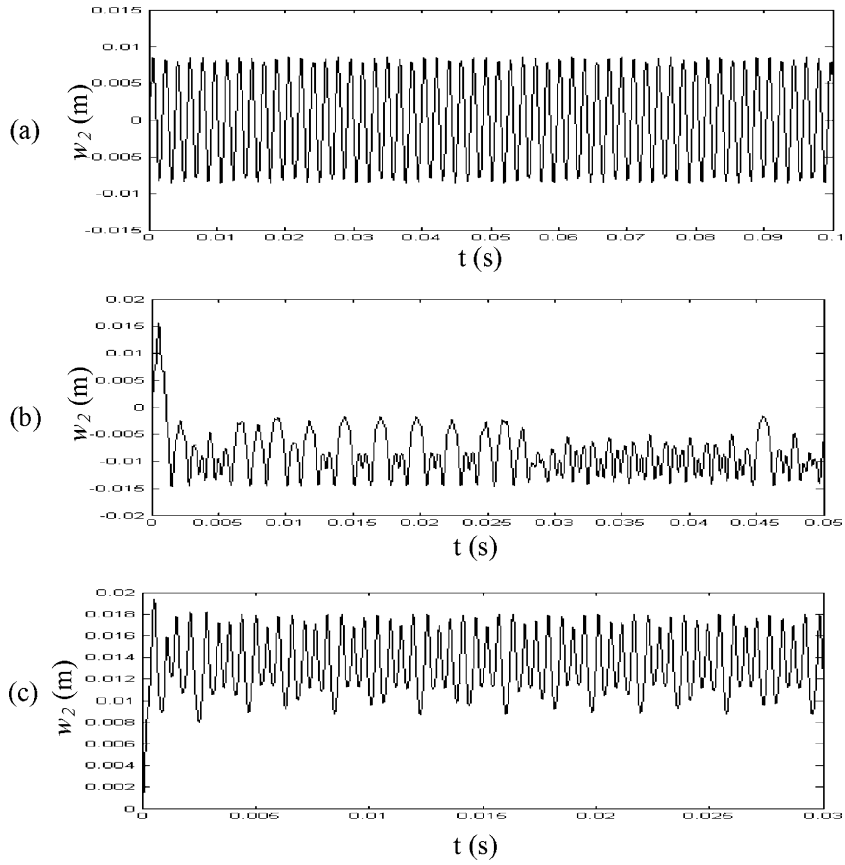

Fig. 2. Displacement–time histories at the midpoint: (a) 1000 N (elastic); (b) 2800 N; (c) 4000 N.

(1991). It will be shown that the present 3-DoF model is capable of demonstrating the asymmetrical responses of elastic–plastic beam.

The asymmetrical responses of an elastic–plastic beam to short pulse load have never been addressed in the existing analytical and numerical approaches. For ideal deterministic structures, the response can be uniquely determined by the system parameters and external loads. However, for engineering structures, geometric or material imperfections may cause uncertainties of the system parameters, and subsequently affect the structural response. On the other hand, the external environment may influence the system response through perturbation such as initial conditions or external loads. In this section, the effect of a very small initial misalignment on the response is studied. This perturbation is applied by assigning a small initial value to w_3, i.e. $w_{30} = 0.001$ mm, which is about 0.037% of the thickness or 0.0005% of the length of the beam. The initial values for w_1 and w_2 remain zero.

Fig. 3(a)–(e) compare the displacement–time histories at the left-quarter point B (w_1) and the right-quarter point D (w_3) with different magnitudes of the short pulse. The magnitudes of the impulsive load are respectively (a) 1000 N, (b) 2500 N, (c) 2800 N, (d) 4200 N and (e) 4400 N. In case (a) of $P = 1000$ N, the displacement–time histories of w_1 and w_3 are almost same, which indicates that the response of the system is approximately symmetrical and insensitive to the small perturbation. The response is purely elastic in this case, implies that such small perturbation could be neglected for the elastic vibration. For cases (b)–(e), plastic strains in the sandwiched cells are relatively high, the displacement–time histories of w_1 and w_3

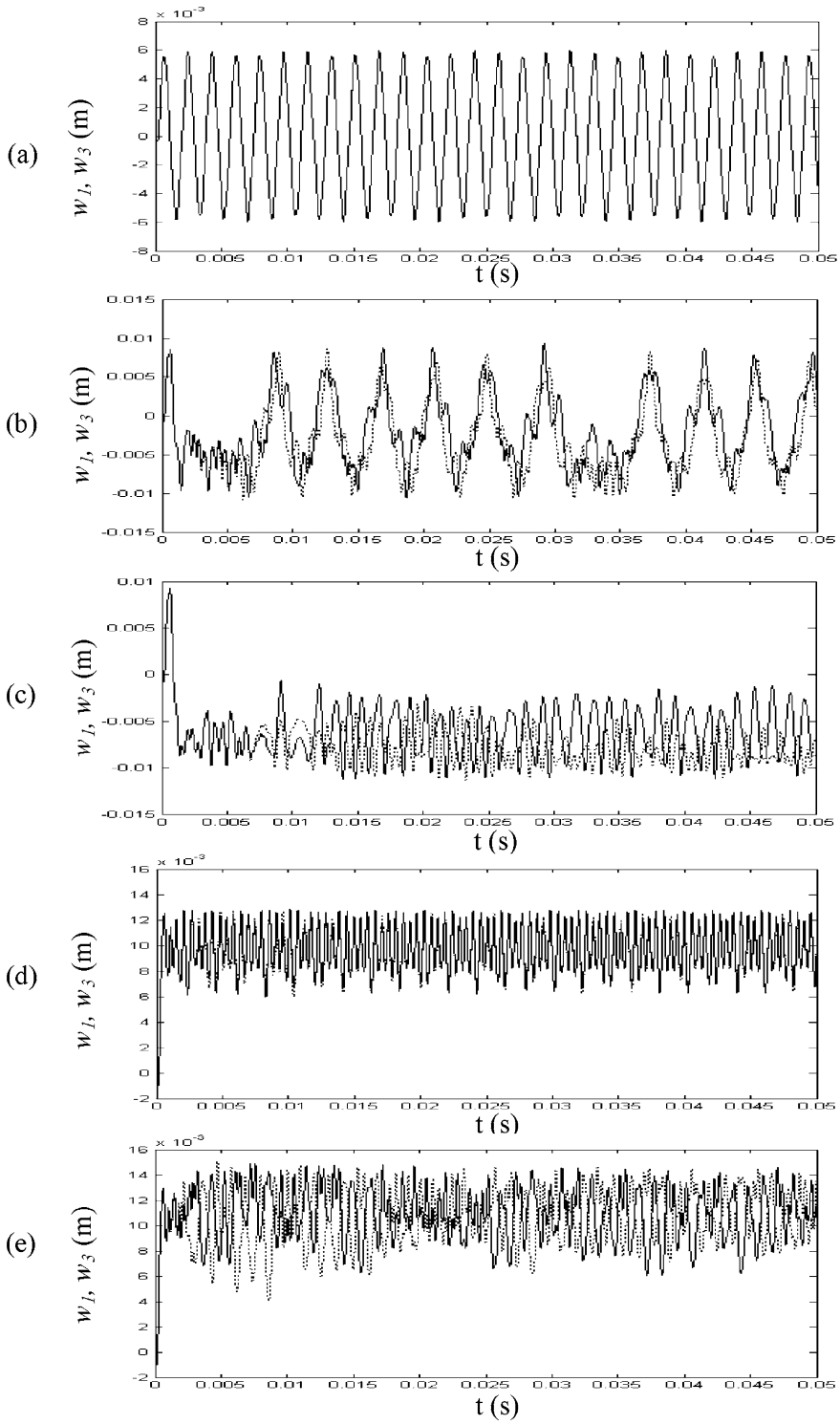

Fig. 3. Displacement–time histories at the left- and right-quarter points: (a) 1000 N; (b) 2500 N; (c) 2800 N; (d) 4200 N; (e) 4400 N. (···) w_1; (—) w_3.

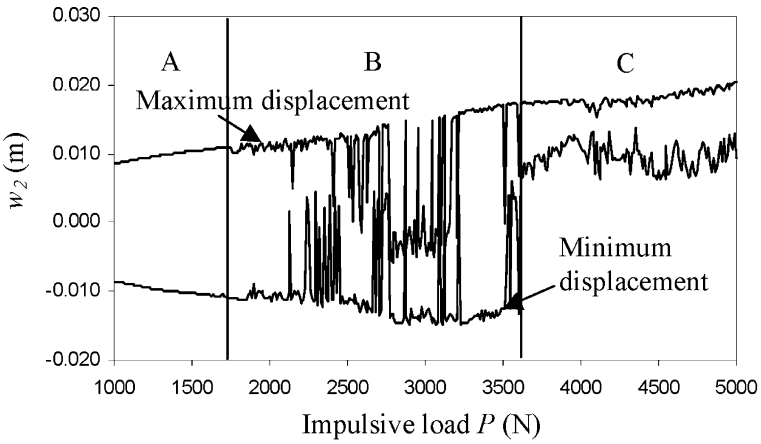

Fig. 4. Characteristic diagram of midpoint displacement w_2.

deviate from each other to different degrees, which means that the 3-DoF system response becomes asymmetrical and sensitive to the initial perturbation. The small perturbation also induces phase shift. For the symmetrical response, w_1 and w_3 always have the same phase. For cases (b) and (d), the phase deviation of w_1 and w_3 is minor. However, for cases (c) and (e), w_1 and w_3 vibrate in opposite phases after the initial period.

The characteristic diagram of the midpoint displacement w_2 with respect to the impulsive load P is depicted in Fig. 4, which is categorized into three zones. The figure is obtained through the calculations at an impulsive load interval of 10 N. The upper curve in Fig. 4 represents the maximum values of the midpoint displacement w_2 between 0.01 and 0.05 s, and the lower curve is the minimum values within this period. The response in the initial period till 0.01 s is not included in the evaluation of the maximum and minimum midpoint displacements. Final deformation at the midpoint will thus rest between the two curves if proper viscous damping is introduced. In zone A, the responses are elastic with quasi-periodic vibration. The counter-intuitive response falls into zone B. Similar to the results obtained by Lee et al. (1992), in some of the regions of zone B, the vibration response is unpredictable because of the disorder of the maximum and minimum displacements at the midpoint. In zone C, the midpoint of the beam vibrates in the positive direction and does not rebound to the negative direction after the impulsive load is removed. The characteristic diagram of the midpoint response shown in Fig. 4 agrees well with the results derived by Lee et al. (1992). It implies that the 2-DoF model (Lee et al., 1992) is a special case of the present 3-DoF model. However, the present 3-DoF model is able to simulate the asymmetrical response of the elastic–plastic system.

5. Characterization of chaotic responses

Chaos is a term referring to the motions in deterministic physical and mathematical systems whose time history depends on initial conditions in an extremely sensitive way. Deterministic prediction of these systems is impossible. On the other hand, it has been perceived that a seemingly underlying order exists which suggests some predictable properties of chaotic behavior. Phase plane, Poincaré map, power spectral density, Lyapunov exponent and fractal dimensions are commonly used tools to explore chaotic response (Moon, 1992). In the present study, the first three methods are applied to characterize the chaotic and asymmetrical response of the 3-DoF Shanley-type beam model.

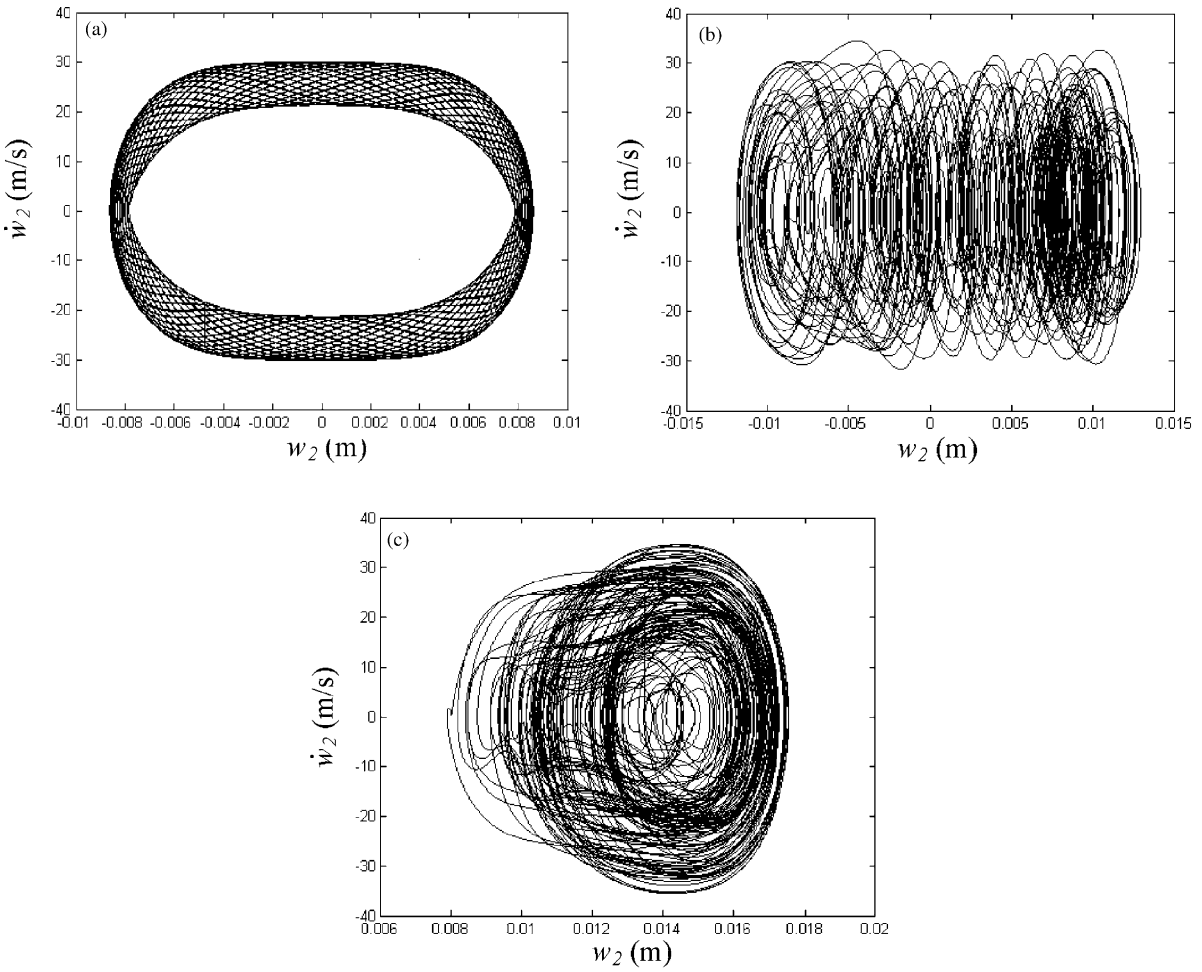

Fig. 5. Phase plane trajectories (midpoint velocity versus displacement): (a) 1000 N; (b) 2500 N; (c) 4400 N.

5.1. Phase plane

Phase plane is defined as a set of points (x, v), where x and v are respectively displacement and velocity variables. Fig. 5 shows the phase plane trajectories with respect to three impulsive loads for the current 3-DoF beam model. When the motion is periodic, the phase plane orbits on closed curves. In Fig. 5(a) with the pulse magnitude 1000 N, the motion is a kind of quasi-periodic. However, in Fig. 5(b) and (c), the traces of motion seem never to overlap, and the trajectories tend to fill up a specific section of the phase space. The casual trace is an implication of chaos, which can be demonstrated more clearly in the modified phase plane called Poincaré map.

5.2. Poincaré map

The motion of a particle is a continuous trajectory in the phase plane. However, if the state of the particle is recorded only at discrete times, the motion will appear as a sequence of points in the phase plane.

When the sampling times are chosen following specific rules, the discrete sampling points construct a Poincaré map. For forced vibration system, if the driving motion has a period of T, the sampling rule for a Poincaré map defines the sampling interval $t_n = nT + \tau_0$, where τ_0 is a starting time of the sampling points. The present 3-DoF Shanley-type beam model is an autonomous system, where the force does not depend explicitly on time. The stroboscopic times are defined as t_i such that $\dot{w}_2(t_i) = 0$, and the Poincaré map is plotted as $w_3(t_i)$ against $w_1(t_i)$. Same method was employed by Lee and Symonds (1992) and Lee et al. (1992).

Fig. 6 shows the Poincaré maps with respect to the three magnitudes of the impulsive force P, i.e. (a) 1000 N, (b) 2500 N and (c) 4400 N. The quasi-periodic motion with $P = 1000$ N is represented by two short segments illustrated in Fig. 6(a). For the chaotic cases (b) and (c), the Poincaré maps do not demonstrate either a finite set of points or a closed orbit. The unorganized points do not form a pattern but appear as a cloud in the map. For case (b), the unorganized points distribute in a narrow band bounded by two lines $w_3 = w_1 + \varepsilon_1$ and $w_3 = w_1 + \varepsilon_2$. For case (c), the two bounding lines can be expressed as $w_3 = -w_1 + \varepsilon_3$ and $w_3 = -w_1 + \varepsilon_4$. $\varepsilon_1, \varepsilon_2, \varepsilon_3$ and ε_4 can be calculated approximately by curve fitting of the boundary points. From the Poincaré maps, it is seen that w_1 and w_3 are phase sensitive. They are in the same phase for case (b), but in the opposite phase for case (c), respectively as shown in Fig. 6(b) and (c).

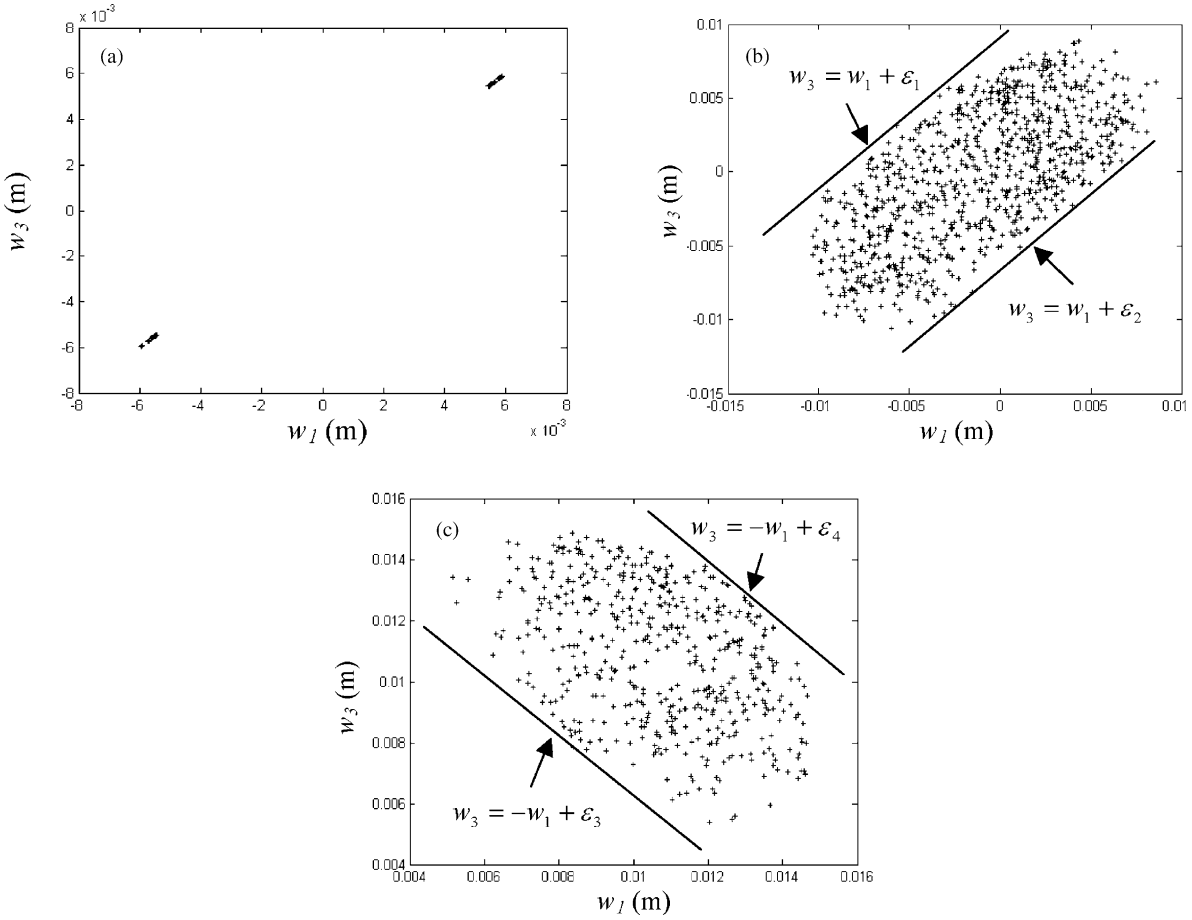

Fig. 6. Poincaré maps: (a) 1000 N; (b) 2500 N; (c) 4400 N.

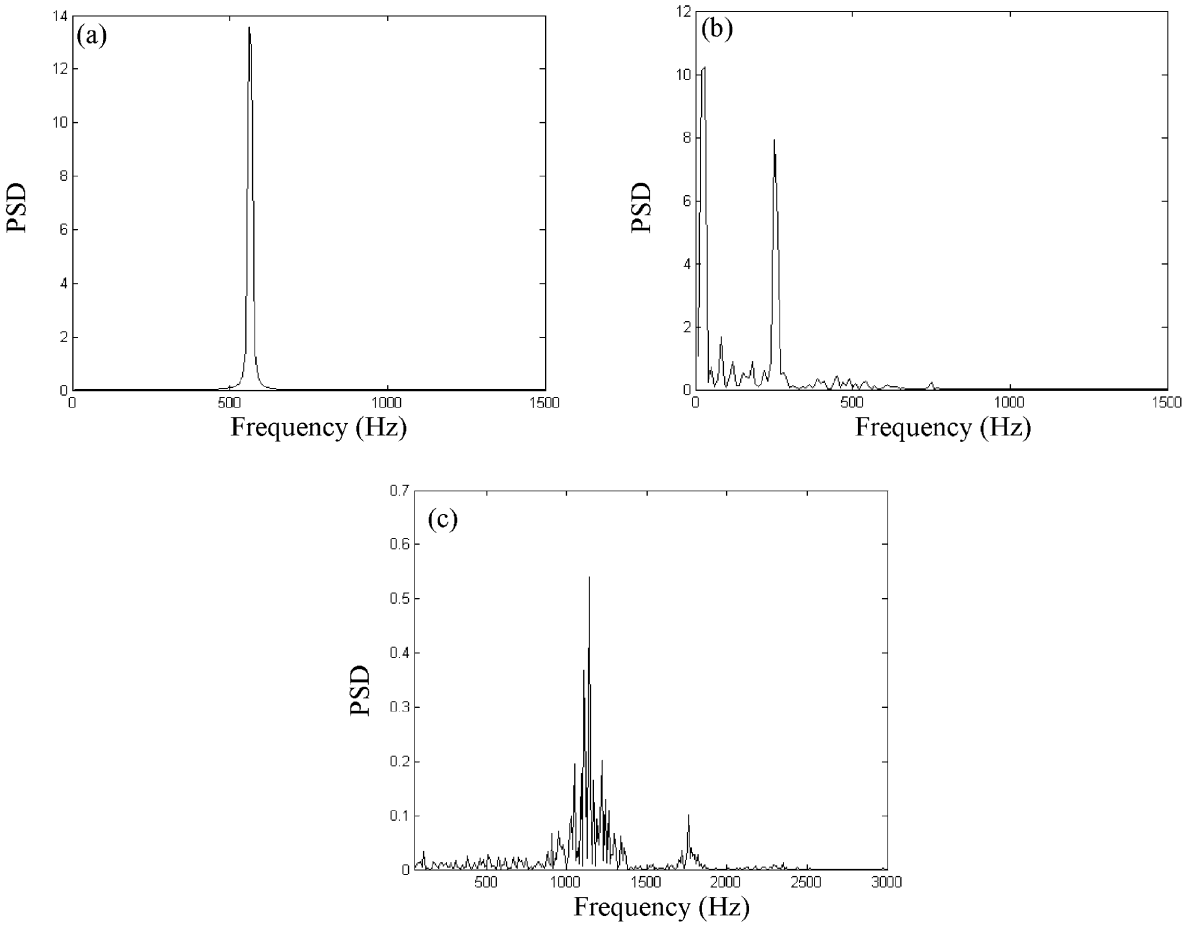

Fig. 7. Power spectral density (PSD) diagrams for impulsive load P: (a) 1000 N; (b) 2500 N; (c) 4400 N.

5.3. Power spectral density

Power spectral density is another important indicator of chaotic response. The change from regular to chaotic vibrations is represented by a change from a power density spectrum consisting of a few isolated peaks at certain frequencies to a much more complicated spectrum, including both broad spectrum and irregular peaks and valleys.

Fig. 7 gives the power spectral density diagrams obtained from fast Fourier transform of the midpoint displacement–time histories. Fig. 7(a) depicts a typical spectrum of regular (quasi-periodic) vibrations. There exists an obvious peak at around 580 Hz in Fig. 7(a), while the energy in Fig. 7(b) and (c) is distributed over a wide range of frequencies, indicating a fully developed chaotic vibration.

6. Effect of vibration modes

Mode superposition is commonly used to calculate the response of systems of finite extent subjected to instant loads (Constantine, 1994). The uncoupled equations of motion are defined by modal participation

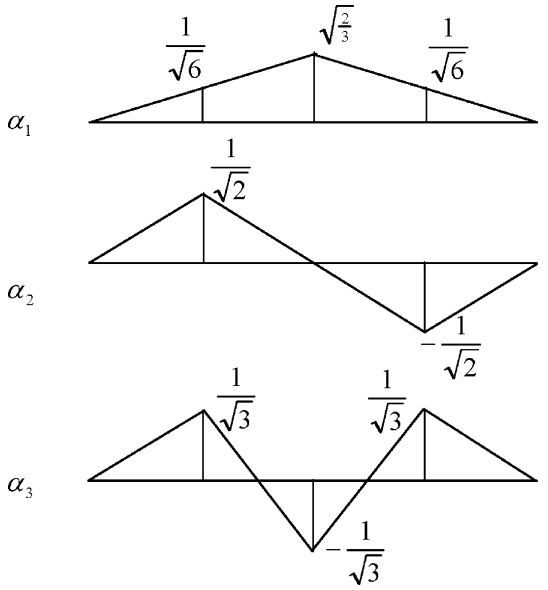

Fig. 8. Vibration modes of the 3-DoF Shanley-type beam model.

factors of each mode. The modal participation factors change with different loads, which consequently determine the variation of the system response.

The concept 'vibration mode' and 'modal participation factor' are extended to the current system for characterizing the chaotic symmetrical and asymmetrical response. Instead of solving the response from the mode shapes and the modal participation factors, the present study determines the modal participation factors through inverse derivation of the displacement response obtained from the central finite difference method. Three orthogonal and normalized mode shapes are defined for the 3-DoF system as shown in Fig. 8. The three modal participation factors α_1, α_2 and α_3 are governed by the three displacement variables. As seen in Fig. 8, the second mode represents an anti-symmetrical vibration mode. The corresponding modal participation factor α_2 characterizes the asymmetrical response of the beam model.

From Fig. 8, the displacement variables w_1, w_2 and w_3 are superposed as

$$\begin{Bmatrix} w_1 \\ w_2 \\ w_3 \end{Bmatrix} = \begin{bmatrix} \frac{1}{\sqrt{6}} & \frac{1}{\sqrt{2}} & \frac{1}{\sqrt{3}} \\ \sqrt{\frac{2}{3}} & 0 & -\frac{1}{\sqrt{3}} \\ \frac{1}{\sqrt{6}} & -\frac{1}{\sqrt{2}} & \frac{1}{\sqrt{3}} \end{bmatrix} \begin{Bmatrix} \alpha_1 \\ \alpha_2 \\ \alpha_3 \end{Bmatrix} \tag{16}$$

The modal participation factors can thus be obtained from Eq. (16) as

$$\begin{Bmatrix} \alpha_1 \\ \alpha_2 \\ \alpha_3 \end{Bmatrix} = \begin{bmatrix} \frac{1}{\sqrt{6}} & \frac{1}{\sqrt{2}} & \frac{1}{\sqrt{3}} \\ \sqrt{\frac{2}{3}} & 0 & -\frac{1}{\sqrt{3}} \\ \frac{1}{\sqrt{6}} & -\frac{1}{\sqrt{2}} & \frac{1}{\sqrt{3}} \end{bmatrix}^{-1} \begin{Bmatrix} w_1 \\ w_2 \\ w_3 \end{Bmatrix} \tag{17}$$

Fig. 9 shows the time histories of the modal participation factors in the first 0.05 s of response time. In all the five cases, α_1 has the largest magnitude comparing with α_2 and α_3, which implies that the first mode always dominates the vibration. In case (a) with P is equal to 1000 N, the amplitude of α_2 approximates zero in the concerned response time period. Therefore, the response of the system is mainly symmetrical. In the

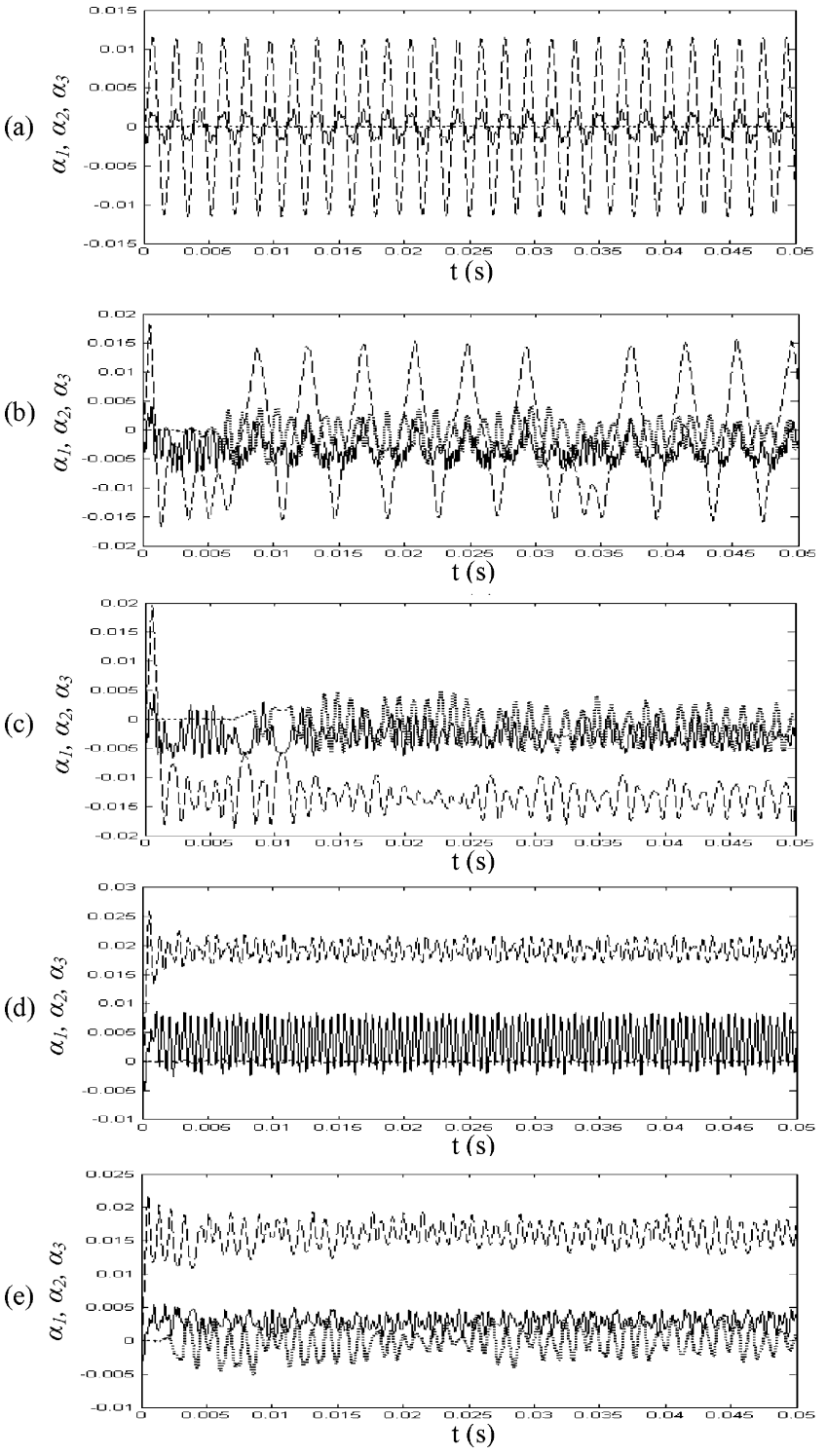

Fig. 9. Time histories of modal participation factors: (a) 1000 N; (b) 2500 N; (c) 2800 N; (d) 4200 N; (e) 4400 N. (---) α_1; (···) α_2; (—) α_3.

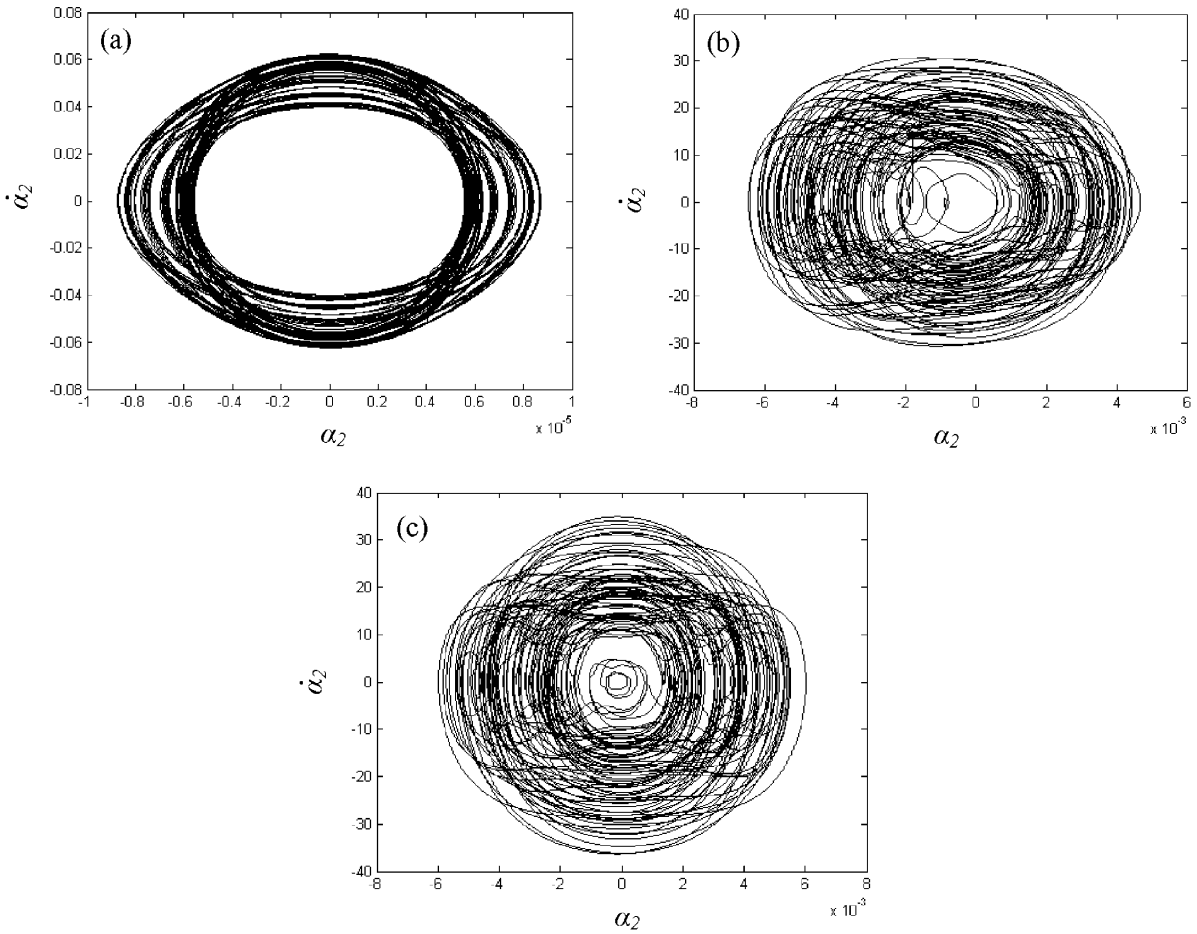

Fig. 10. Phase plane trajectories of α_2: (a) 1000 N; (b) 2500 N; (c) 4400 N.

other cases, the anti-symmetrical mode is activated and the modal participation factor α_2 holds zero only in a very short initial period, after which it starts to contribute to the system response, and consequently results in the asymmetrical vibration. The effect of α_2 is anomalous because it may vanish in certain pulse magnitude as illustrated in Fig. 9(d).

The phase plane trajectories of α_2 are plotted in Fig. 10 for the three different impulsive loads, i.e. (a) 1000 N, (b) 2500 N, (c) 4400 N. It is observed that the quasi-periodic vibration with $P = 1000$ N forms a close phase plane trajectory of the modal participation factor α_2. The two chaotic cases, however, derives non-overlapped traces on the α_2 phase plane. Fig. 11 illustrates the Poincaré maps of the modal participation factors for the same three cases as illustrated in Fig. 10. The stroboscopic times are defined as instants t_i such that $\dot{\alpha}_2(t_i) = 0$, and the Poincaré maps are plotted as $\alpha_3(t_i)$ against $\alpha_1(t_i)$. It is seen again that the quasi-periodic motion with $P = 1000$ N produces a regular pattern of the Poincaré map (see Fig. 11(a)). However, the Poincaré maps with $P = 2500$ and 4400 N as illustrated respectively in Fig. 11(b) and (c) by the unorganized points show obvious chaotic characteristics. Fig. 12 depicts the power spectral density diagrams obtained from the time histories of α_2 for the three cases. The chaotic spectrum of the asymmetrical vibration can be clearly identified from the wide range distribution of energy in the frequency

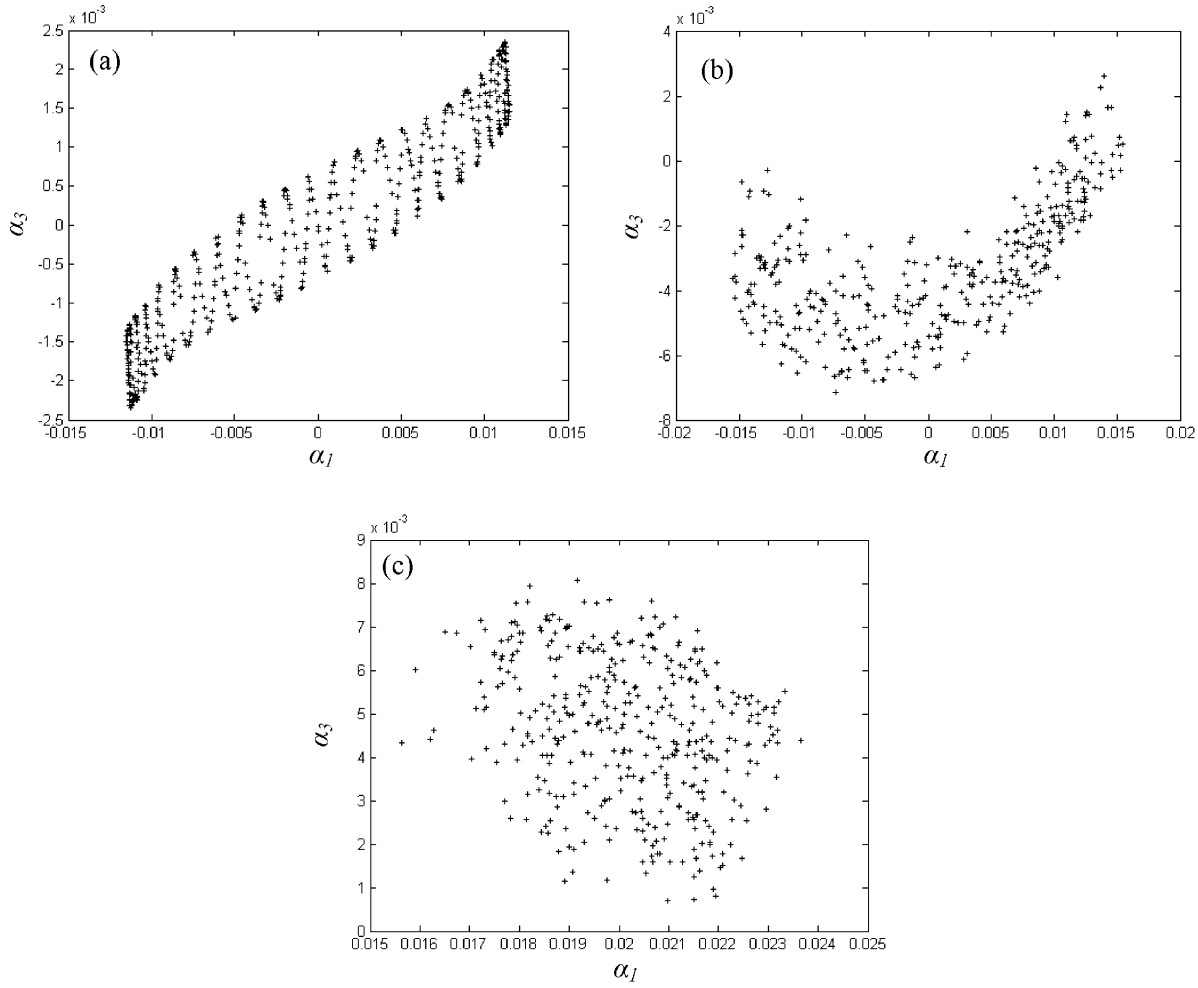

Fig. 11. Poincaré maps of modal participation factors: (a) 1000 N; (b) 2500 N; (c) 4400 N.

domain (see Fig. 12(b) and (c)). The quasi-periodic vibration, however, is dominated by a single peak vibration frequency, which is much higher than the symmetrical elastic vibration frequency (about 580 Hz). From Figs. 10–12, it can be recognized that, if the magnitude of the impulsive load is relatively low, the modal participation factors vibrates quasi-periodically and the effect of the asymmetrical mode is very minor. However, with increase of the magnitude of the load, the beam model exhibits obvious chaotic characteristics for both symmetrical and asymmetrical vibration responses.

The characteristic diagram of the modal participation factors with impulsive load varying from 1000 to 5000 N is shown in Fig. 13, calculated again with a pulse magnitude interval of 10 N. The duration of the rectangular pulse is kept 0.5 ms. The modal participation factors in the diagram are defined as the maximum absolute value within 0.02 s of vibration period. It is seen that the modal participation factor α_1 increases steadily with the increase of the impulsive load P. The third modal participation factor α_3 representing the second order symmetrical vibration mode also has an ascending trend although there are a few minor descending regions. The ascending trend indicates that the modal participation factors α_1 and α_3 become larger with the increase of the impulsive load. It is reasonable because the beam model responds

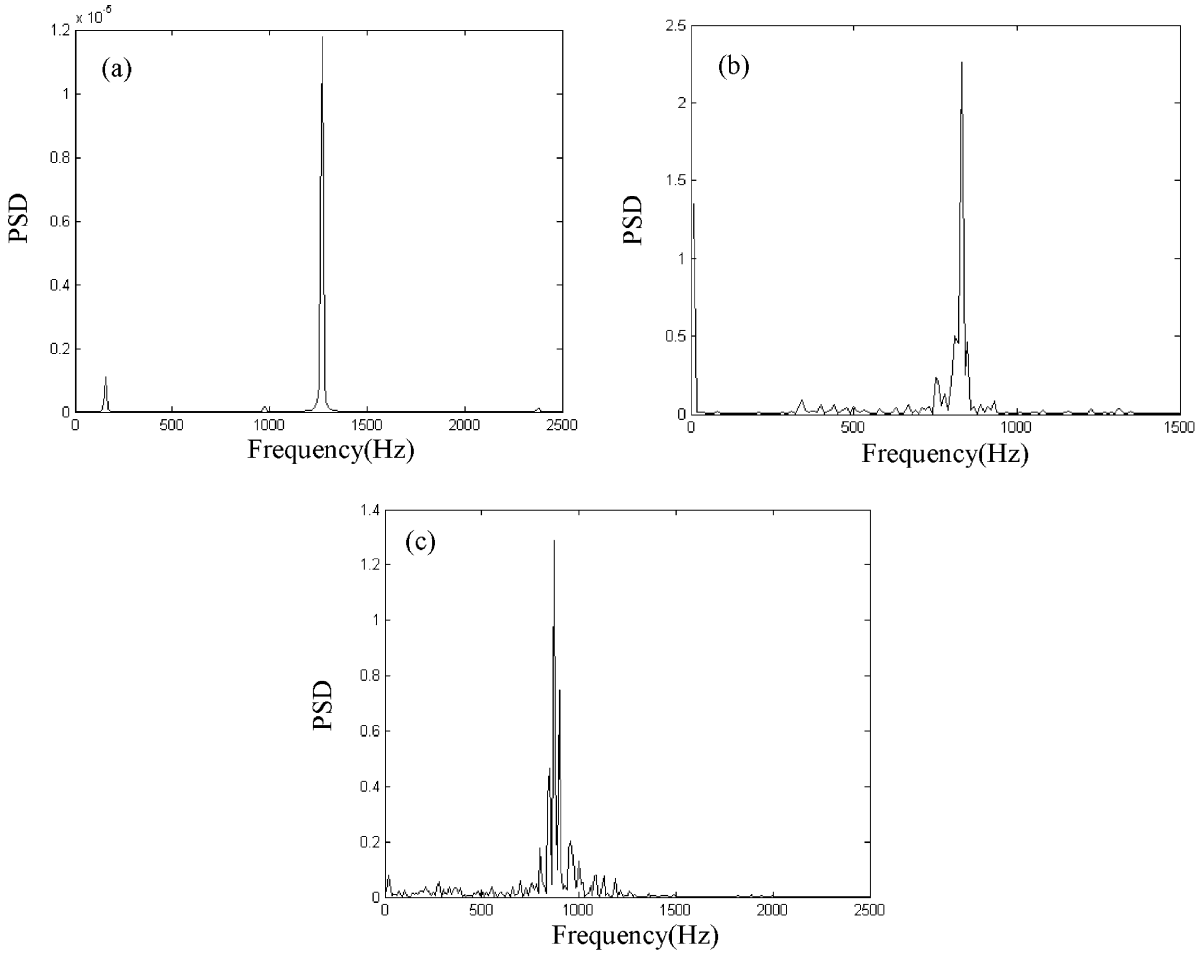

Fig. 12. Power spectral density (PSD) diagrams of α_2: (a) 1000 N; (b) 2500 N; (c) 4400 N.

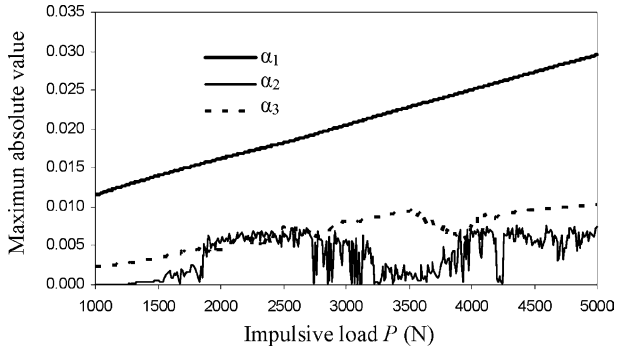

Fig. 13. Characteristic diagram of the modal participation factors.

more significant symmetrical displacement with the increase of the external impulsive load. The second modal participation factor α_2 changes sharply after the impulsive load exceeds a critical value about 1500 N. Besides, the maximum absolute value of α_2 is very sensitive to the applied load, indicating that the asymmetrical response of the system is anomalous. There exist several narrow regions of the impulsive load within which α_2 are approximately zero.

7. Numerical simulation of asymmetrical response for elastic–plastic beam

To further address the asymmetrical response of elastic–plastic beams, the uniform beam model employed by Symonds and Lee (1992) with both ends fully constrained is analyzed using a general-purpose FE code LS-DYNA (2001). A concentrated force with a rectangular pulse of intensity P and duration $t_0 = 0.5$ ms is applied at the midpoint of the beam. The material of the beam is elastic, perfectly plastic. The span, the width and the thickness of the beam are 203.2, 20 and 2.32 mm respectively. The Young's modulus, the yielding stress, the mass density and the Poisson's ratio of the beam material are taken as 70 GPa, 0.3 GPa, 2700 kg/m^3 and 0.3, respectively.

To activate asymmetrical response of the beam, very small misalignment is assigned to the beam as shown in Fig. 14. Points A and E are the two fixed-ends of the beam. Point B, C and D are the left-quarter point, the midpoint and the right-quarter point of the beam, respectively. w_0 is the initial misalignment at point B with a value of 0.01 mm, which results in an initial rotation angle α approximating 0.01°.

The uniform beam is meshed with $200\times20\times5$ brick elements. The elastic and kinematic plastic hardening material model *MAT_PLASTIC_KINEMATIC in LS-DYNA is adopted. The simulated displacement–time histories at the points B, C and D with respect to different magnitudes of the short pulse load are shown in Fig. 15. It is seen that the beam vibrates symmetrically when the magnitude of the short pulse is relatively small (Fig. 15(a) and (b)) because of the almost identical displacement variations at points B and D. Asymmetrical response occurs when the applied load is 1300 N. However, it vanishes when the load is 1600 N. For cases (b) and (c), the beam behaves counter-intuitively. The simulation results confirm again that the asymmetrical response is sensitive to the applied load. Fig. 16 plots the difference between the displacement–time histories at the left-quarter point B (w_B) and the right-quarter point D (w_D). The analytical and numerical results in the present study conform to the experimental observations of Li et al. (1991).

8. Conclusions

A three-degree-of-freedom beam model is developed, which is capable of capturing the asymmetrical response of elastic–plastic beams. The main purpose of the present paper is to present basic features of the asymmetrical counter-intuitive response mode, which has been observed in previous experiment (Li et al., 1991), but were ignored in past investigations. There exist other issues, which are worthy for further studies, e.g., using the energy method (Borino et al., 1989; Lee and Symonds, 1992; Lee et al., 1992) to study the

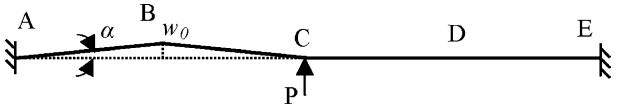

Fig. 14. Initial misalignment of fix-ended beam.

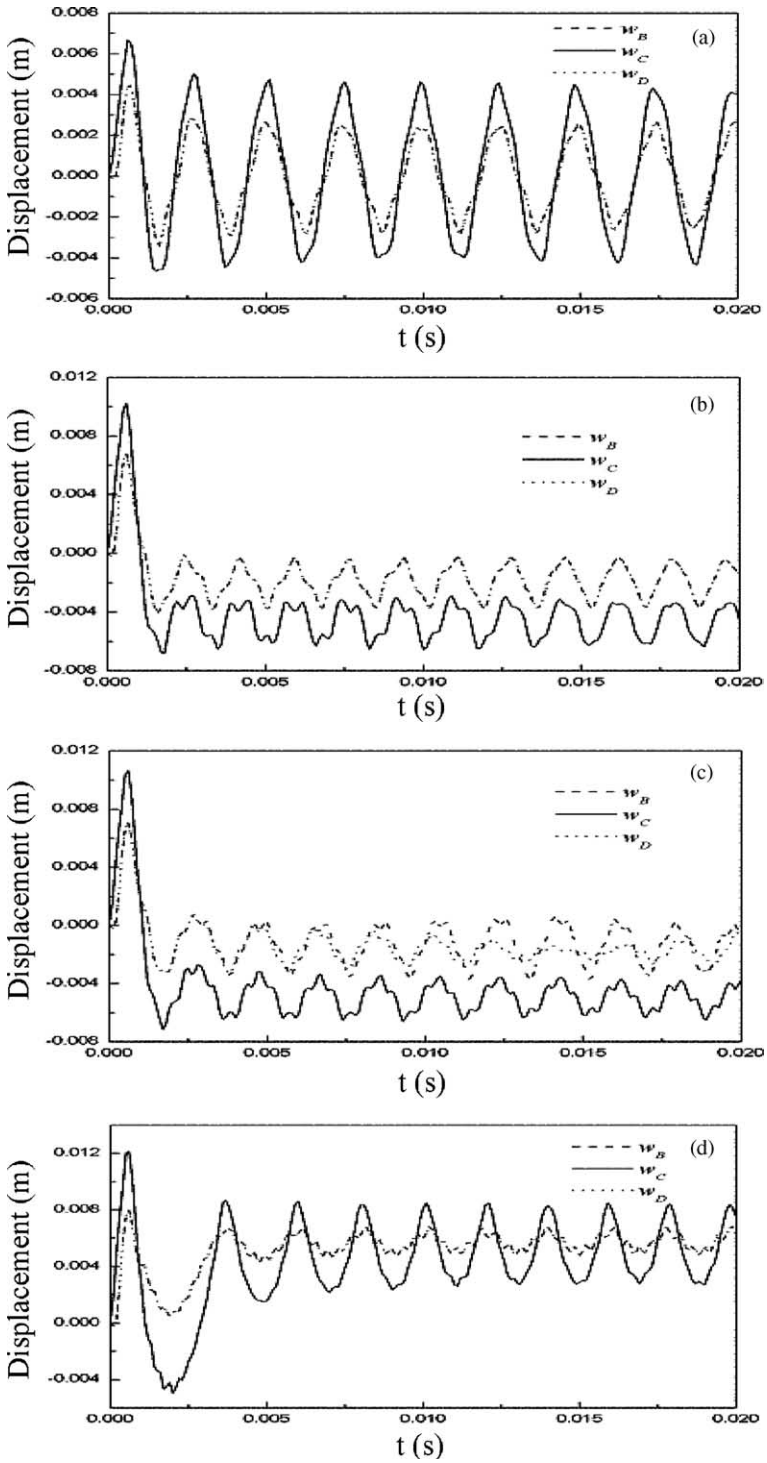

Fig. 15. Displacement–time histories at points B, C and D: (a) 600 N; (b) 1200 N; (c) 1300 N; (d) 1600 N.

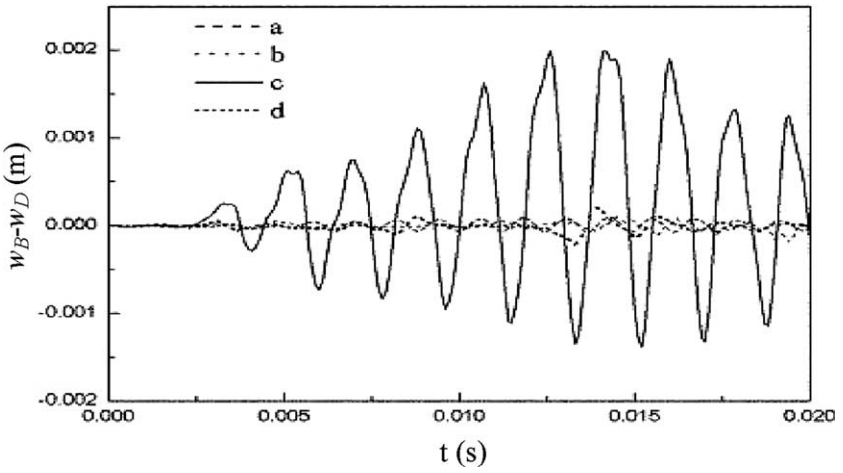

Fig. 16. Difference between the displacement–time histories at points B and D: (a) 600 N; (b) 1200 N; (c) 1300 N; (d) 1600 N.

response boundary of the 3-DoF beam model. However, the complexity of the topography of the strain energy surface will increase due to the increase of degree of freedom.

The two-degree-of-freedom Shanley-type model (Lee et al., 1992) is a special case of the present model. Through decomposition of the vibration response, asymmetrical vibration of the elastic–plastic beam model is identified. Both the symmetrical and the asymmetrical vibrations are chaotic. The asymmetrical vibration becomes significant when the impulsive load exceeds a critical value. The asymmetrical vibration may be interpreted as the second-order chaotic response of elastic–plastic beam, whereas the well-addressed counter-intuitive behavior is the first order chaos. For the 3-DoF model, same parameters as those used by Lee et al. (1992) were employed in order to validate our results. However, for the FE model, the parameters adopted by Symonds and Lee (1992) were used in order to compare present results from LS-DYNA with the previous results using ABAQUS. It is shown that present results are capable of duplicating the results in the previous studies and revealing the asymmetric responses of the beam.

Experiment data of the asymmetrical final deformation is very limited and scattered. The present study did not compare the analytical results with the experimental data quantitatively. To accurately capture the asymmetrical and chaotic final deformation of an elastic–plastic beam, more experiment data with careful setup of impact tests are required.

The present analytical Shanley-type model is able to capture the basic features of the chaotic and asymmetrical response of elastic–plastic beam. It provides guidance for numerical simulations and experimental studies of the chaotic beam response under short pulse load.

References

Bassi, A., Genna, F., Symonds, P.S., 2002. Anomalous elastic–plastic responses to short pulse loading of circular plates. International Journal of Impact Engineering 28, 65–91.

Borino, G., Perego, U., Symonds, P.S., 1989. An energy approach to anomalous damped elastic–plastic response to short pulse loading. ASME Journal of Applied Mechanics 56, 430–438.

Constantine, S., 1994. Finite Element Modeling in Engineering Practice: Includes Examples with ALGOR. West Virginia University Press, Morgantown, West Virginia.

Galiev, Sh.U., 1996. Experimental observations and discussion of counterintuitive behavior of plates and shallow shells subjected to blast loading. International Journal of Impact Engineering 18 (7–8), 783–802.

Galiev, Sh.U., 1997. Influence of cavitation upon anomalous behavior of a plate/liquid/underwater explosion system. International Journal of Impact Engineering 19 (4), 345–359.

Genna, F., Symonds, P.S., 1987. Induced vibrations and dynamic instabilities of a nonlinear structural model due to pulse loading. Meccanica 22, 144–149.

Kolsky, H., Rush, P., Symonds, P.S., 1991. Some experimental observations of anomalous response of fully clamped beams. International Journal of Impact Engineering 11 (4), 445–456.

Lee, J,Y., Symonds, P.S., 1992. Extended energy approach to chaotic elastic–plastic response to impulsive loading. International Journal of Mechanical Science 34 (2), 139–157.

Lee, J.Y., Symonds, P.S., Borino, G., 1992. Chaotic response of a two-degree-of-freedom elastic–plastic beam model to short pulse loading. ASME Journal of Applied Mechanics 59, 711–721.

Li, Q.M., Liu, Y.M., 2003. Uncertain dynamic response of a deterministic elastic–plastic beam. International Journal of Impact Engineering 28, 643–651.

Li, Q.M., Zhao, L.M., Yang, G.T., 1991. Experimental results on the counter-intuitive behavior of thin clamped beams subjected to projectile impact. International Journal of Impact Engineering 11 (3), 341–348.

Livermore Software Technology Corporation, 2001. LS-DYNA Keyword User's Manual, Version 960. Vol. 1–2, Livermore, CA, USA.

Moon, F.C., 1992. Chaotic and Fractal Dynamics: An Introduction for Applied Scientists and Engineers. John Wiley and Sons, Inc., New York.

Qian, Y., Symonds, P.S., 1996. Anomalous dynamic elastic–plastic response of a Galerkin beam model. International Journal of Mechanical Science 38 (7), 687–708.

Symonds, P.S., Lee, J.Y., 1992. Anomalous and unpredictable response to short pulse loading. In: Hui, D., Jones, N. (Eds.), Recent Advances in Impact Dynamics of Engineering Structures, AMD 105. ASME, New York, pp. 31–38.

Symonds, P.S., Yu, T.X., 1985. Counterintuitive behavior in a problem of elastic–plastic beam dynamics. ASME Journal of Applied Mechanics 52, 517–522.

Symonds, P.S., McNamara, J.F., Genna, F., 1986. Vibrations and permanent displacements of a pin-ended beam deformed plastically by short pulse excitation. International Journal of Impact Engineering 4, 73–82.